Heliyon 10 (2024) e35594

Contents lists available at ScienceDirect

Heliyon

journal homepage: www.cell.com/heliyon

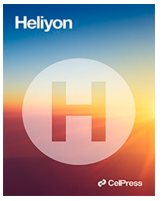

Research article

Effect of MgO/ZnO ratio on the formation process of $Mg_xZn_{1-x}O$ ceramics

N. Korsunska [a], Yu. Polishchuk [a], S. Ponomaryov [a], K. Kozoriz [a], S. Chusnutdinow [b,c], O. Melnichuk [d], L. Melnichuk [d], L. Khomenkova [a,e,*]

[a] V. Lashkaryov Institute of Semiconductor Physics at the National Academy of Sciences of Ukraine, Kyiv, Ukraine
[b] Institute of Physics, Polish Academy of Sciences, Warsaw, Poland
[c] International Research Center MagTop, Institute of Physics, Polish Academy of Sciences, Warsaw, Poland
[d] Mykola Gogol Nizhyn State University, Nizhyn, Ukraine
[e] National University "Kyiv-Mohyla Academy", Kyiv, Ukraine

ARTICLE INFO

Keywords:
(Mg,Zn)O solid solution
Diffusion
Doping
SEM
Auger electron spectroscopy
Luminescence
Defects

ABSTRACT

The structural characteristics, chemical composition, and element spatial distribution in $Mg_xZn_{1-x}O$ ceramics were investigated using X-ray diffraction, scanning electron microscopy, Auger electron spectroscopy, energy-dispersive X-ray spectroscopy, and cathodoluminescence techniques. The study revealed that the morphology of the ceramic samples, as well as the mechanism of solid solution formation, depend on the relative contribution of both oxides in the charge. It was discovered that hexagonal and cubic phases of the solid solution were found to form simultaneously. An increase in the MgO content in the charge results in the magnesium content rise in the hexagonal grains continuously, reaching approximately 13 at.%. It was discovered an enrichment of grain boundaries with zinc and magnesium playing a significant role in doping ZnO and MgO grains. Obtained results allowed to propose two mechanisms involved in the formation of solid solution ceramics: i) diffusion of Mg and Zn along grain boundaries, followed by their incorporation into ZnO or MgO grains, respectively, and ii) interdiffusion of Mg into ZnO and Zn into MgO due to direct contact of ZnO and MgO grains. The second mechanism appears to dominate when both ZnO and MgO contribute comparably, increasing the probability of their direct contact. This study significantly advances the understanding of the process of the formation of $Mg_xZn_{1-x}O$ ceramics under thermodynamic conditions. These insights are crucial for optimizing the doping process and improving the material properties, thereby promoting innovations in the ceramics industry.

1. Introduction

Metal oxides and their solid solutions demonstrate a number of unique properties that determine their wide application in electronics, medicine, photonics, various sensors, and radiation detectors. Currently, ZnO occupies an important place as a promising material for photodetectors, transparent electrodes, varistors, and gas sensors [1]. To expand the scope of its application in optoelectronic devices to the ultraviolet region of the spectrum, ZnO is doped with magnesium. It changes the electrical conductivity,

* Corresponding author. V. Lashkaryov Institute of Semiconductor Physics at the National Academy of Sciences of Ukraine, Kyiv, Ukraine.
E-mail addresses: korsunska@ukr.net (N. Korsunska), khomen@ukr.net (L. Khomenkova).

https://doi.org/10.1016/j.heliyon.2024.e35594
Received 24 May 2024; Received in revised form 11 July 2024; Accepted 31 July 2024
Available online 2 August 2024

especially in the films and pressed nanopowders [2,3], which is promising for developing *p*-type materials.

Due to the inconsistency of the crystal structure of hexagonal ZnO and cubic MgO, these oxides do not form a continuous series of solid solutions under thermodynamic conditions. Besides, due to the limited solubility of Mg in ZnO and Zn in MgO, the range of the existence of solid solutions with a hexagonal or cubic structure only is also limited. It should be noted that the solubility values of the components differ greatly. In particular, Mg solubility in ZnO varies from 4 at.% [4] up to 33 at.% [5] and even up to 70 at.% [6] that depends on the sample preparation approach. Higher Mg solubility in the hexagonal phase was observed in the films with a metastable structure grown under non-equilibrium conditions. Contrary to this, samples obtained under thermodynamic equilibrium show much lower Mg solubility in ZnO (10 at.% at 1645°C [7] or 14 at.% at 1000°C [8]).

Among the methods of solid solution preparation under equilibrium conditions, the solid-phase reaction is often considered for the $Mg_xZn_{1-x}O$ preparation via the sintering of ZnO and MgO powders taking in the required ratio. In such a case, ceramic samples can simultaneously include hexagonal and cubic phases of a solid solution. This allows estimating the Mg content in the hexagonal phase and the Zn content in the cubic phase as well as their interrelation with the ratio of MgO and ZnO in the initial charge. For instance, in Ref. [9], the Mg content in the hexagonal phase was found to be ~17 at.% at 1600°C being lower than in the films.

Solid state sintering is attractive for the preparation of $Mg_xZn_{1-x}O$ solid solutions due to its simplicity, and low cost. It has the potential for modifying the characteristics of the samples via impurity introduction into the initial charge [10], the presence of boundaries between hexagonal and cubic phases, or the inhomogeneous distribution of components within the grains of one phase. At the same time, the processes of the formation of different phases were studied insufficiently. In particular, the distribution of components across the grains, between different grains and at grain boundaries, the morphology of samples versus ZnO and MgO ratio in the charge, the influence of Zn and/or Mg evaporation, and so on. Some of these processes were considered for ceramics of a certain composition. In particular, in Ref. [11], the possibility of ZnO evaporation was assumed for $Mg_xZn_{1-x}O$ with $x = 0.1$ and 0.6, whereas EDS analysis of ceramics sintered at 600–1100 °C showed the statistical variation of Mg content in the samples. This was explained by the high oxygen pressure in the ambient atmosphere that inhibited Zn evaporation. However, the EDS sensitivity towards zinc is limited to about 0.5 at.% meaning hardly possible detection of the evaporation of Zn with a smaller amount. In Ref. [12], for $Mg_xZn_{1-x}O$ with $x = 0.05$, 0.1 and 0.2, it was also suggested that MgO could evaporate and precipitate on the sample surface, which was used for explanation of the short-wavelength shift of the absorption edge during the sintering of ceramics in a sealed ampoule. However, to the author knowledge, a detailed study of the dependence of the morphology of $Mg_xZn_{1-x}O$ ceramic samples and the distribution of the Zn and Mg elements depending on the contribution of ZnO and MgO, when it changes over a wide range, has not been performed. At the same time, such studies can be useful for elucidating the mechanisms of solid solution ceramic formation.

Therefore, in this paper, the influence of the content of ZnO and MgO in the charge on the structural characteristics of $Mg_xZn_{1-x}O$ ceramic samples, and the distribution of components in ceramics, including different grains and grain boundaries, were investigated.

2. Experimental details

The samples were formed from a mixture of ZnO and MgO powders of submicron sizes (200–300 nm), taken in the appropriate ratio x calculated from $(MgO)_x(ZnO)_{1-x}$ formula. The purity of ZnO and MgO powders was 99.99 % and 99.97 %, respectively. For each sample, the desired mole fractions of the powders were taken and the mixture was then cold-pressed at a pressure of 50 MPa. After that, the samples were annealed in air at a temperature of 1100 °C for 3 h and cooled with a furnace.

X-ray diffraction was measured in the Bragg-Brentano (Θ-2Θ) geometry with a PhilipsX'Pert-MRD diffractometer using $Cu_{K\alpha 1}$ radiation with a wavelength of 0.15406 nm. Scanning electron microscopy (SEM), Auger electron spectroscopy (AES), and energy dispersive X-ray spectroscopy (EDX) were used to study the morphology and element distribution in ceramic grains. The measurements

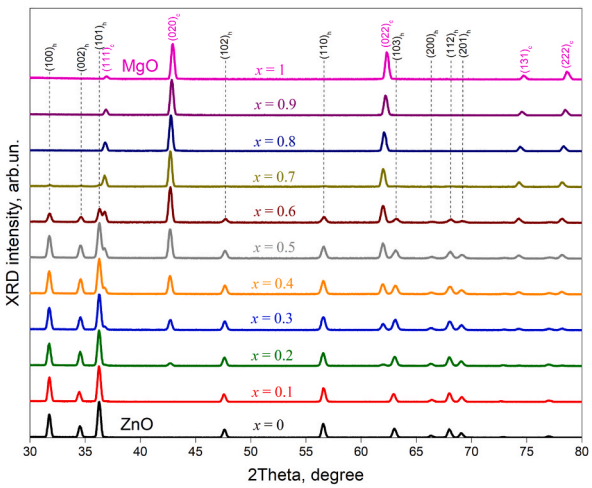

Fig. 1. XRD patterns of different $Mg_xZn_{1-x}O$ solid solutions. The curves are shifted vertically for clarity.

were performed using JAMP-9500F Field Emission Auger microprobe (JEOL). The spatial resolution in the secondary electron image mode was 3 nm. The microprobe was equipped with a sensitive hemispheric Auger spectrometer with energy resolution ΔE/E from 0.05 to 0.6 % and an ion etching gun for layer-by-layer analysis with a diameter of Ar + ion beam 120 μm, able to move by raster 1 × 1 mm^2. The variation range of the beam Ar + ion energy is from 0.01 to 4 keV, while the minimal beam current is 2 μA with 3 keV. To obtain chemical maps by EDX and AES methods, preliminary etching with Ar ions was used to remove about a 100-nm surface layer and to clean the samples from contaminations. For the analysis, the AES signals in the range of O KLL (481.0–526.0 eV), Zn LMM (971.0–1002.0 eV) and Mg KLL (1163.0–1198.0 eV) transitions were used. The chemical composition was determined from the AES signals by the method of relative sensitivity factors using the approach described in Ref. [16] and taken into account the AES and EDX data of the initial MgO and ZnO powders. All measurements were performed at room temperature.

Cathodoluminescence (CL) was studied using SEM ZEISS EVO HD15 - HORIBA Jobin Yvon CLUE system. The SEM chamber is equipped with a parabolic mirror for the collection of the CL signal. The detection system consists of a 320 mm monochromator (HORIBA iHR320) equipped with 600 groves/mm grating and a connected CCD camera (Synapse HORIBA Jobin Yvon). All CL maps were done at the temperature of 300 K, by using a beam accelerating voltage and the probe current, 20 kV and 1 nA respectively.

3. Results

3.1. XRD study of $Mg_xZn_{1-x}O$ ceramics

The XRD patterns of the samples with different compositions are shown in Fig. 1 along with the data for ZnO and MgO ones. For the ZnO ceramics, the diffraction peaks from the $(100)_h$, $(002)_h$, $(101)_h$, $(102)_h$, $(110)_h$, $(103)_h$, $(200)_h$, $(112)_h$ and $(201)_h$ family planes are in the agreement with ICDD card # 96-230-0451. For the MgO ceramics, the XRD peaks are ascribed to the $(111)_c$, $(020)_c$, $(022)_c$, $(131)_c$ and $(222)_c$ family planes (ICDD card # 96-900-7059).

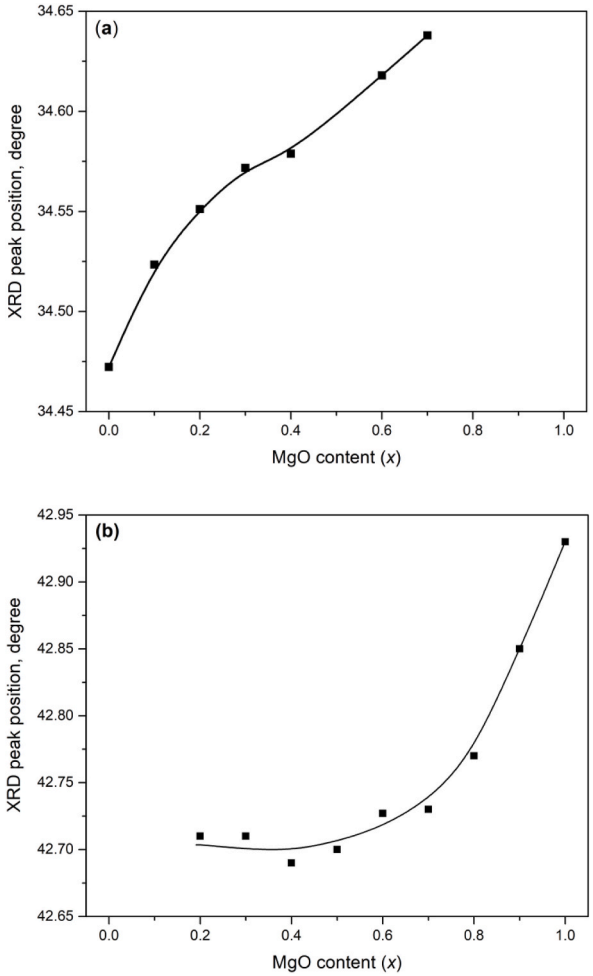

Fig. 2. Effect of MgO content in the charge (x) on the peak position of $(002)_h$ XRD reflex of hexagonal phase (a) and $(020)_c$ XRD reflex of the cubic phase (b) of the solid solution.

The analysis of the XRD patterns of the ceramics with different Mg content shows that for samples with $x = 0.1$ only hexagonal peaks are observed, whereas for $0.2 \leq x \leq 0.7$, both hexagonal and cubic peaks are detected. In the samples with $x \geq 0.8$, only cubic phase is registered.

The analysis of the XRD peak positions revealed that the Mg content increase results in the shift of the position of the $(002)_h$ peak of the hexagonal phase to the larger angles compared to the $(002)_h$ peak of pure ZnO, which indicates the incorporation of the Mg into ZnO and the formation of the hexagonal phase of the solid solution [9]. Along with this, the $(020)_c$ peak of the cubic phase is shifted towards smaller angles in comparison with that of pure MgO, supporting the formation of the cubic phase of the solid solution. The corresponding dependencies of the angle positions of the $(002)_h$ and $(020)_c$ peaks versus the x values are shown in Fig. 2. It can be seen that an increase in the magnesium content up to $x = 0.7$ leads to a continuous shift of the $(002)_h$ peak position of hexagonal phase (Fig. 2,a). This means that the solubility limit of Mg in ZnO was not reached even for the highest MgO content as $x = 0.7$. At the same time, the cubic phase of the solid solution appears for $x = 0.2$ showing a significant shift of the $(020)_c$ peak position towards $2\Theta \sim 42.72^\circ$ in comparison with that of MgO ($2\Theta \sim 42.93^\circ$) cubic phase (Fig. 2,b). This shift is more pronounced when x decreases from 1.0 down to 0.7. For low Mg content, it becomes smaller, and for $x = 0.2$–0.5, the position of the $(020)_c$ XRD peak changes slightly. This could mean that the solubility limit of the Zn in MgO was approached.

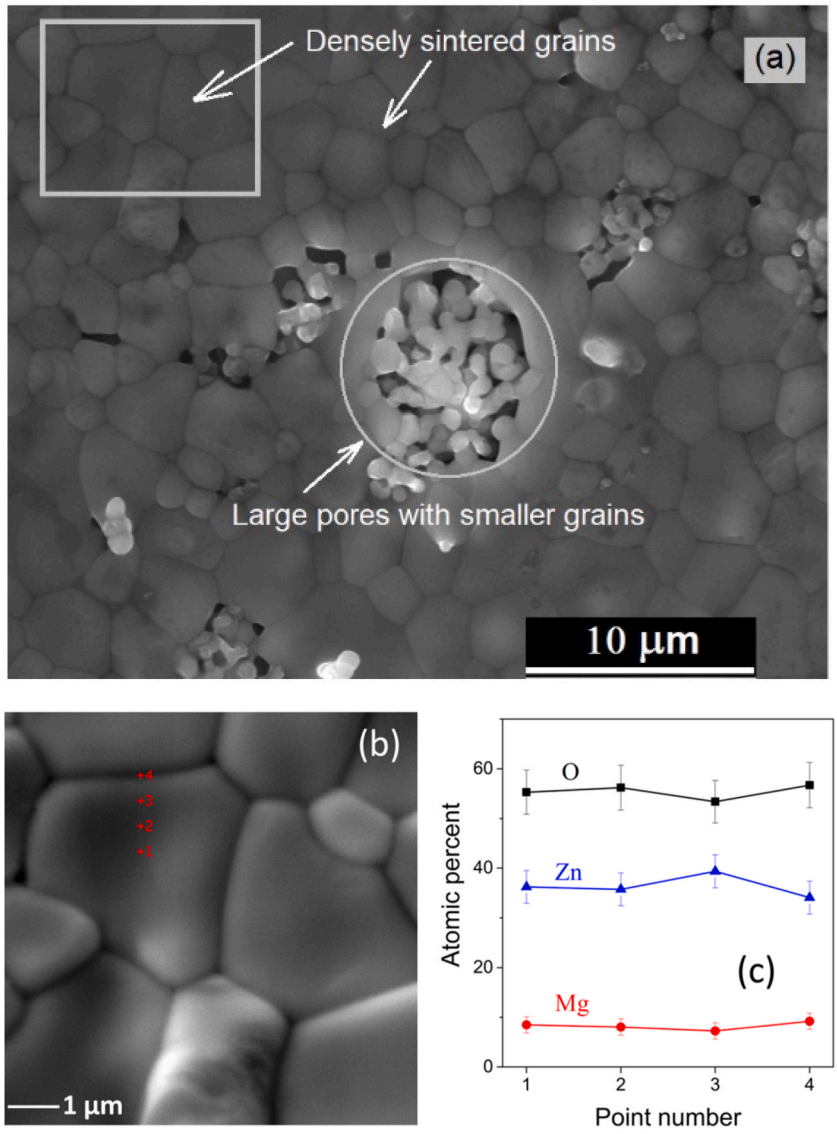

Fig. 3. SEM image of the surface of the $Mg_{0.2}Zn_{0.8}O$ sample (a) and the area with densely sintered grains (highlighted with grey box) is enlarged in (b). The chemical composition of densely sintered grains obtained by Auger electron spectroscopy is shown in (c).

3.2. SEM study, Auger electron and EDX spectroscopy

A characteristic feature of ceramics, regardless of its composition, is the higher grain sizes in comparison with the particle sizes of the raw powders. However, its morphology and distribution of components depend on the MgO content. The most specific samples were submitted for detailed structural characterization along with the analysis of chemical composition distribution.

3.2.1. $Mg_{0.2}Zn_{0.8}O$ ceramics

In the samples with $x = 0.1–0.2$, an array of densely sintered grains of the hexagonal phase is formed (Fig. 3,a). In some cases, the large pores containing grains of somewhat smaller sizes appear on the ceramic surface (Fig. 3,a). An enlarged image of the surface area with densely sintered grains is presented in Fig. 3,b along with the corresponding Zn, Mg and O distribution determined from the AES spectra (Fig. 3,c). At the glance, the distribution of the Mg content in densely sintered grains varies slightly along the grain (points 1–4) whereas the Zn content significantly exceeds the Mg content, which corresponds to the hexagonal phase of the solid solution. However, the detailed analysis of element distribution in the area of densely sintered grains revealed a decrease in the Zn content near the grain boundaries and an increase in the Zn and Mg concentration at the grain boundaries, as evidenced by the AES maps shown in Fig. 4. The comparison of the AES maps for Zn and Mg (Fig. 4) with the map for O (Fig. 1S) testifies to the segregation of the metal ions at the grain boundaries followed by their possible subsequent oxidation.

The grains in the pores are significantly different from the densely sintered grains. As can be seen from Fig. 5, they are of other shapes and show the growth steps. The magnesium content in these grains is much higher than in densely sintered ones (Fig. 5b). Besides, the zinc content can noticeably increase near their boundaries. Since the magnesium content in these grains exceeds its solubility in ZnO [7,8], it can be assumed that the grains in the pores correspond to the cubic phase of the solid solution, the presence of which in the sample is confirmed by XRD data.

The EDX study of the grains shows that the magnesium content in various grains of the hexagonal phase varies within 5–6 at.% and does not depend significantly on the distance to the pore. At the same time, the zinc content in most grains in the pores is 15–19 at.%, but in some of them, located near the boundary of the pore, it can reach 29 at.%. In the latter case, obviously, one cannot draw a conclusion about their structure. Note that the samples also contain a small amount of carbon (Fig. 5,b).

3.2.2. $Mg_{0.4}Zn_{0.6}O$ ceramics

The morphology of $Mg_{0.4}Zn_{0.6}O$ samples was found to be similar to the morphology of $Mg_{0.2}Zn_{0.8}O$ samples (Fig. 1S). The areas with densely sintered grains and pores including grains with higher magnesium content similar in shape were also observed. The content of magnesium in densely sintered grains in $Mg_{0.4}Zn_{0.6}O$ according to EDX data increases slightly compared to its content in the sample $Mg_{0.2}Zn_{0.8}O$. As for Zn content in the grains located in the pores, it also depends on grain location, being somewhat lower than that for $Mg_{0.2}Zn_{0.8}O$ samples (11–14 at.% for the grain located in the pore center and 25–26 at.% in the grains located near their boundaries). In the area of densely sintered grains, the grain boundaries are also enriched with zinc and magnesium with Mg being a bit higher compared to $Mg_{0.2}Zn_{0.8}O$ sample.

3.2.3. $Mg_{0.5}Zn_{0.5}O$ ceramics

A further increase in the content of magnesium oxide, when the contribution of ZnO and MgO becomes comparable, significantly changes the morphology of ceramics. As can be seen from Fig. 6, which shows the image of the surface area of the $Mg_{0.5}Zn_{0.5}O$ sample, densely sintered grains of different compositions are observed in the ceramics.

As evidenced by EDX data, these grains differ greatly in magnesium content. In some of them, the magnesium content is about 35 at.%, and in other ones, it is ~7–9 at.%, i.e. these grains obviously correspond to the cubic and hexagonal phases, respectively. The grains of the cubic phase, as in the case of lower MgO content, show growth steps which is not observed in the grains of the hexagonal phase.

It should be noted that, as evidenced by EDX and AES data (Fig. 7), near the boundaries between the grains of both phases, there are regions enriched in zinc or magnesium in the grains of the cubic and hexagonal phases, respectively (Fig. 7, b). Simultaneously, the AES map demonstrates corresponding regions of Zn depletion in hexagonal grains and Mg depletion in cubic ones near the boundaries where they are in contact (Fig. 8). An increased Mg and Zn concentration at the grain boundaries in the arrays of grains of the same phase is also observed in these samples as in the samples with $x = 0.2–0.4$ values.

3.2.4. $Mg_{0.8}Zn_{0.2}O$ ceramics

With a further increase in MgO content in the charge, the number of grains of the hexagonal phase decreases, while sintering

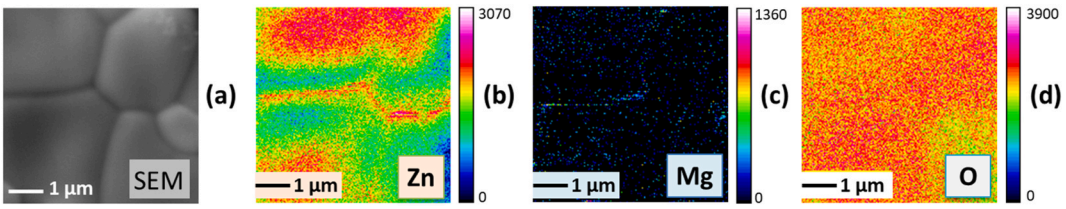

Fig. 4. SEM image of the surface area (a) and AES maps for Zn (b), Mg (c) and O (d) distribution in $Mg_{0.2}Zn_{0.8}O$ ceramics.

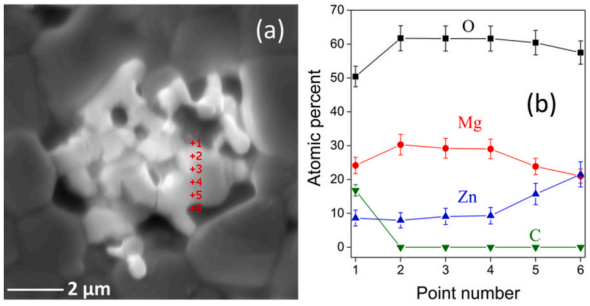

Fig. 5. SEM image of a large pore (a) and the distribution of elements in the crystallites located in the pores, obtained from the Auger electron spectra (b) in the $Mg_{0.2}Zn_{0.8}O$ sample.

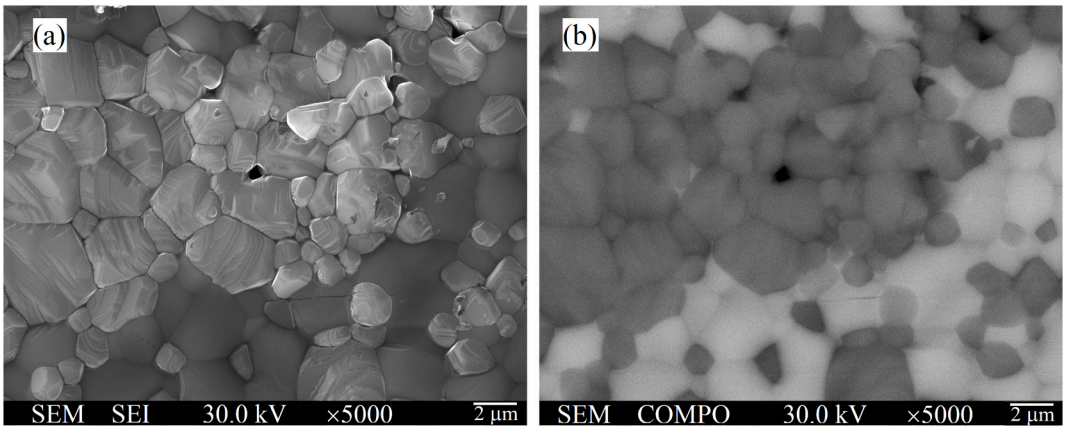

Fig. 6. SEM images taken in secondary electron mode (a) and compositional mode (b) for the surface of the $Mg_{0.5}Zn_{0.5}O$ sample.

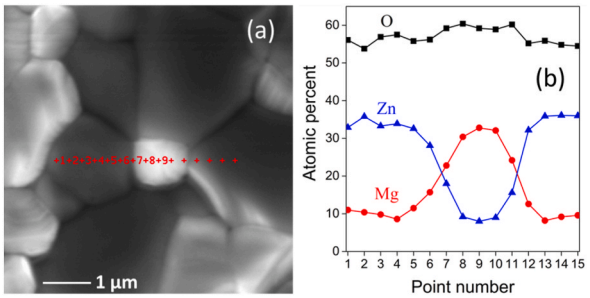

Fig. 7. SEM image of the surface showed the presence of the hexagonal (dark) and cubic (bright) grains (a) and the distribution of elements (b) in the $Mg_{0.5}Zn_{0.5}O$ sample.

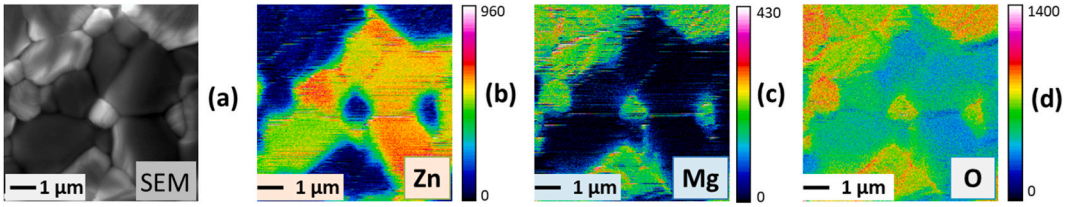

Fig. 8. SEM COMPO image of the surface area of the $Mg_{0.5}Zn_{0.5}O$ sample (a) with corresponding Zn (b), Mg (c) and O (d) AES maps.

worsens (a large number of small pores appear). At $x \geq 0.8$, grains of the hexagonal phase are not observed, which correlates with the disappearance of the corresponding reflexes in the XRD patterns (Fig. 1). At the same time, the enrichment of intergranular boundaries with zinc and magnesium is clearly observed, and the grains of the cubic phase are doped homogeneously enough, as in the case of magnesium doping of hexagonal grains in $Mg_{0.2}Zn_{0.8}O$ ceramics (Fig. 9). According to the EDX data, increasing the magnesium oxide content in the charge leads to a gradual increase of Mg content in the hexagonal ceramic grains, which is consistent with the XRD data. When MgO content in the charge increases from $x = 0.2$ to $x = 0.7$, the magnesium content in the grains with a hexagonal structure increases gradually from ~5 to 6 at.% to 8–13 at.%. Therefore, based on the obtained data, it is not possible to draw a conclusion about the solubility limit of magnesium in ZnO in our ceramics.

As for the grains of the cubic phase, the Zn content inside them increases from ~10 at. % to ~16 at.% with a Zn content increase from $1\text{-}x = 0.2$ to 0.5 (i.e. Mg content decreases from $x = 0.8$ to $x = 0.5$), and at the higher ZnO content practically does not change, which correlates with XRD data and may mean approaching the solubility limit of zinc in MgO.

However, this value remains lower than the solubility limit of Zn in MgO reported in the literature (~24 at.% at a temperature of 1000°C [9]). At the same time, as mentioned above, in some regions (mainly contacting with hexagonal grains) zinc content can reach 25 at.%. If they have a cubic structure, the solubility limit of zinc in MgO agrees with the literature data [9]. It can be assumed that the solubility limit may be reached in the near-surface regions of grains.

4. Discussion

As can be seen from the X-ray diffraction data, the shift of the reflexes from hexagonal and cubic phases during ceramic sintering occurs simultaneously, which indicates the simultaneous formation of both phases of the solid solution. This can be explained by the doping of ZnO grains with magnesium and MgO grains with zinc, which can occur simultaneously at the temperature of ceramic sintering. Indeed, ZnO doping with magnesium takes place at temperatures above 700°C [13], and MgO doping with zinc occurs at temperatures above 150°C [14,15], and diffusion can occur from the corresponding oxides. Based on this, it can be supposed that the absence of peaks of the cubic phase at $x \leq 0.1$ and peaks of the hexagonal phase at $x \geq 0.8$ in XRD data can be explained by the complete dissolution of MgO in the grains of the hexagonal phase and ZnO in the grains of the cubic one.

The above presented data also demonstrate that the morphology of $Mg_xZn_{1-x}O$ ceramics depends on the content of magnesium oxide. In particular, at $x \leq 0.4$, the formation of densely sintered grains of the hexagonal phase and large pores with the grains of the cubic one is typical. At the same time, at higher x values ($x \geq 0.4$), densely sintered grains of cubic and hexagonal phases are formed, where the grains of both phases are in contact. In addition, as the x increases, porosity increases (sintering worsens), which is probably due to poor sintering of magnesium oxide grains.

One of the reasons for different morphology may be the increased concentration of zinc and magnesium at the grain boundaries. Enrichment of these boundaries with zinc is probably caused by the process of its evaporation, which is known [16] to take place at temperatures above 800 °C. In such a case, one can expect the presence of metallic Zn and/or Zn oxide. The comparison of the Zn and O distribution in corresponding AES maps allows the presence of Zn oxide at the grain boundaries to be supposed. An additional argument for this statement is the observation of green luminescence with the maximum near 510–530 nm which is a known feature of ZnO [1,17]. As one can see from Fig. 10, the distribution of CL intensity recorded at 530 nm wavelength from the surface of the $Mg_{0.2}Zn_{0.8}O$ sample shows the enhancement of the green emission at the grain boundaries.

The enrichment of intergranular boundaries with magnesium is less pronounced, and the mechanism of its occurrence is not

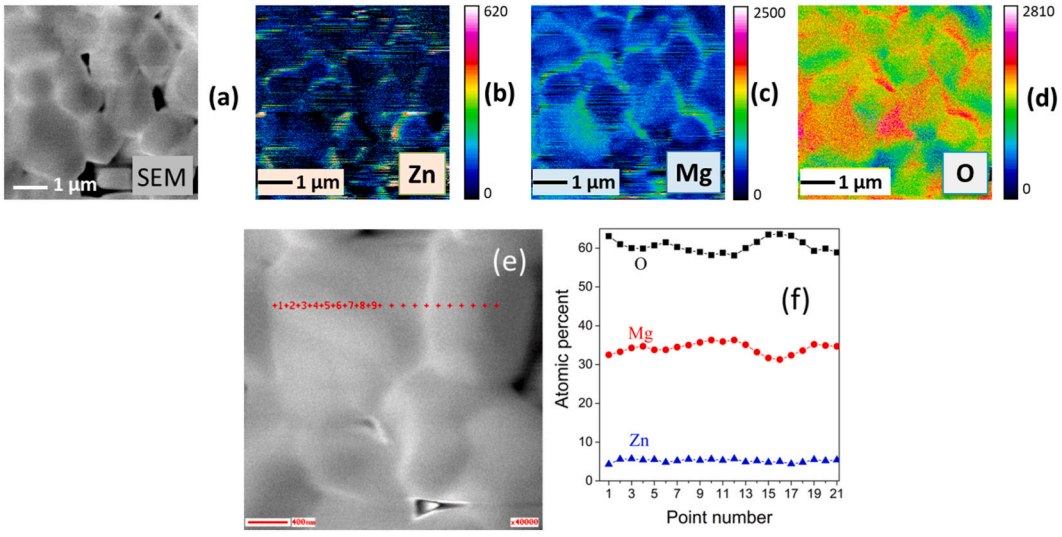

Fig. 9. SEM COMPO image of sample surface (a) with corresponding Zn (b), Mg (c) and O (d) AES maps for $Mg_{0.8}Zn_{0.2}O$ sample. The images (e) and (f) demonstrate a SEM COMPO image of sintered cubic grains (e) and spatial distribution of elements along these grains (f).

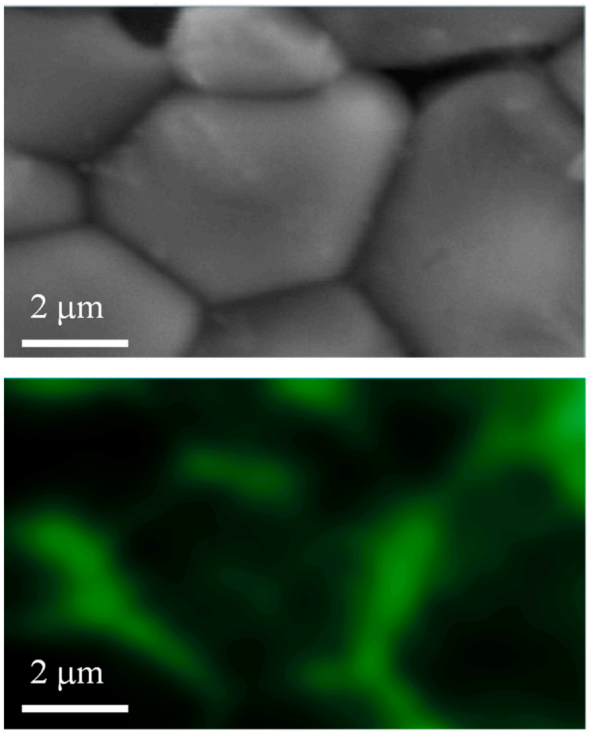

Fig. 10. SEM image of the surface of $Mg_{0.2}Zn_{0.8}O$ sample (upper panel) and corresponding CL map recorded at 530 nm registration wavelength (bottom panel).

entirely clear. One can assume that it can be related, for instance, to the presence of metallic Mg in the initial powder as well as the reduction of MgO in the presence of carbon during sintering.

An increase in the concentration of zinc at the grain boundaries of hexagonal grains can promote their dense sintering and, as a result, the formation of large pores around the grains of the cubic phase, which is observed in the case of $x \leq 0.4$. On the other hand, the release of magnesium and its subsequent melting and oxidation may be the reason for the appearance of growth steps on the grains of the cubic phase and their growth compared to the size of the powder MgO particles. In particular, their shape is polyhedral (octagonal), which is observed in the case of MgO particles' formation due to oxidation of molten magnesium [18].

As evidenced by the above data, the enrichment of grain boundaries with magnesium and zinc can also play an important role in the doping of raw powder particles and the formation of a solid solution. In particular, it can be assumed that the mechanism of the formation of the hexagonal phase of the solid solution at $x \leq 0.4$ may be the diffusion of magnesium released from the MgO particles along these boundaries and its subsequent incorporation into the ZnO lattice. This is supported by the close composition of the grains of the hexagonal phase solid solution, located at a considerable distance from the cubic (MgO-rich) grains. The essential role of diffusion from the boundaries can also be one of the reasons why in the ceramics investigated the solubility limit of Mg in ZnO was not reached. Another reason can be the evaporation of Mg from ceramic sample.

The same situation can take place when MgO particles are doped with zinc at a low content of zinc oxide in the charge. This mechanism of solid solution formation can be dominant for the cubic phase at a low content of ZnO and the hexagonal one at a low content of MgO in the charge, i.e. at the boundaries of the composition interval.

Another situation is realized in the case of comparable contribution of both oxides, when the probability of direct contact of ZnO and MgO particles increases. In this case, the conditions for the diffusion of Mg into ZnO directly from MgO particles and Zn into MgO from ZnO ones are realized. This is evidenced by zinc depletion of hexagonal grains and by magnesium depletion of cubic ones near their boundaries, where they are in contact. This also causes the increased concentration of Mg in hexagonal grains and Zn in cubic grains near their boundaries. Thus, in the case of a comparable contribution of oxides, in addition to doping from intergranular boundaries, the formation of solid solution due to interdiffusion of components at direct contact of ZnO and MgO grains is realized, and, in this case, it can be dominant.

Thus, when $Mg_xZn_{1-x}O$ ceramics are sintered, the hexagonal and cubic phases of the solid solution are formed simultaneously. At the same time, two mechanisms of their formation are observed. One of them is caused by the segregation of zinc and magnesium at the grain boundaries and their subsequent diffusion into MgO and ZnO, respectively, and the second one is associated with the interdiffusion of cations due to the direct contact of MgO and ZnO particles.

5. Conclusion

The structural characteristics, chemical composition, and spatial distribution of elements in $Mg_xZn_{1-x}O$ ceramics of different compositions were investigated using the methods of X-ray diffraction, scanning electron microscopy, Auger electron spectroscopy, energy-dispersive X-ray spectroscopy, and cathodoluminescence. It was found that the morphology of the samples, as well as the mechanism of solid solution formation, depends on the relative contribution of ZnO and MgO. It is shown that the hexagonal and cubic phases of the solid solution are formed simultaneously, as evidenced by the shift of the corresponding X-ray diffraction reflexes. According to these data and EDX ones the Mg content in the hexagonal ceramic grains continuously increases up to ~13 at.%, with the increase of MgO content in the charge i.e., in ceramics prepared under the used sintering conditions the solubility limit of magnesium in ZnO is not reached, being higher 13 at.%.

Enrichment of grain boundaries with zinc and magnesium was revealed. It was concluded that this plays an important role in doping of the raw oxide particles and affects the morphology of the samples. It is proposed that the formation mechanism of the solid solution at a low content of ZnO or MgO in the charge can be the diffusion of magnesium and zinc along the grain boundaries and their subsequent incorporation into ZnO or MgO. Under comparable contribution of both oxides, when the probability of contact of ZnO and MgO grains increases, the dominant mechanism of solid solution formation can be the direct diffusion of Mg into ZnO and Zn into MgO from corresponding oxide particles.

CRediT authorship contribution statement

N. Korsunska: Writing – review & editing, Writing – original draft, Validation, Supervision, Formal analysis, Conceptualization. **Yu. Polishchuk:** Writing – review & editing, Visualization, Software, Resources, Investigation, Formal analysis, Data curation. **S. Ponomaryov:** Writing – review & editing, Visualization, Software, Resources, Investigation, Formal analysis, Data curation. **K. Kozoriz:** Writing – review & editing, Visualization, Investigation. **S. Chusnutdinow:** Writing – review & editing, Visualization, Validation, Resources, Formal analysis, Data curation. **O. Melnichuk:** Writing – review & editing, Visualization, Validation, Resources, Project administration, Formal analysis, Conceptualization. **L. Melnichuk:** Writing – review & editing, Visualization, Investigation, Data curation. **L. Khomenkova:** Writing – review & editing, Visualization, Validation, Supervision, Project administration, Investigation, Data curation, Conceptualization.

Declaration of competing interest

The authors declare that they have no known competing financial interests or personal relationships that could have appeared to influence the work reported in this paper.

Acknowledgements

This work was supported by the National Academy of Sciences of Ukraine as well as by the National Research Foundation of Ukraine from the state budget, project 2020.02/0380 «Structure transformation and non-equilibrium electron processes in wide bandgap metal oxides and their solid solutions». The research in Poland was supported by the National Science Centre (Grant No. 2021/41/B/ST3/03651) and partially by the Foundation for Polish Science through the IRA Programme co-financed by the EU within SG OP (Grant No. MAB/2017/1).

Appendix A. Supplementary data

Supplementary data to this article can be found online at https://doi.org/10.1016/j.heliyon.2024.e35594.

References

[1] Ü. Özgür, Ya I. Alivov, C. Liu, A. Teke, M.A. Reshchikov, S. Doğan, V. Avrutin, S.-J. Cho, H. Morkoç, A comprehensive review of ZnO materials and devices, J. Appl. Phys. 98 (2005) 041301, https://doi.org/10.1063/1.1992666.
[2] Wanjun Li, Liang Fang, Guoping Qin, Haibo Ruan, Hong Zhang, Chunyang Kong, Lijuan Ye, Ping Zhang, Fang Wu, Tunable zinc interstitial related defects in ZnMgO and ZnCdO films, J. Appl. Phys. 117 (2015) 145301, https://doi.org/10.1063/1.4917207.
[3] Y. Ke, S. Lany, J.J. Berry, J.D. Perkins, P.A. Parilla, A. Zakutayev, T. Ohno, R. O'Hayre, D.S. Ginley, Enhanced electron mobility due to dopant-defect pairing in conductive ZnMgO, Adv. Funct. Mater. 24 (2014) 2875–2882, https://doi.org/10.1002/adfm.201303204.
[4] E.R. Segnit, A.E. Holland, The system MgO-ZnO-SiO_2, J. Am. Ceram. Soc. 48 (1965) 409–413, https://doi.org/10.1111/j.1151-2916.1965.tb14778.x.
[5] A. Ohtomo, M. Kawasaki, T. Koida, K. Masubuchi, H. Koinuma, Y. Sakurai, Y. Yoshida, T. Yasuda, Y. Segawa, $Mg_xZn_{1-x}O$ as a II–VI widegap semiconductor alloy, Appl. Phys. Lett. 72 (1998) 2466–2468, https://doi.org/10.1063/1.121384.
[6] D. Thapa, J. Huso, J. Lapp, N. Rajabi, J.L. Morrison, M.D. McCluskey, Thermal stability of ultra-wide-bandgap MgZnO alloys with wurtzite structure, J. Mater. Sci. Mater. Electron. 29 (2018) 16782–16790, https://doi.org/10.1007/s10854-018-9772-y.
[7] B.J. Wuensch, T. Vasilos, Diffusion of Zn^{2+} in single-crystal MgO, J. Chem. Phys. 42 (1965) 4113–4115, https://doi.org/10.1063/1.1695903.
[8] G. Gupta, Sh Verma, R. Nagarajan, Sh Rath, Microstructural and bandgap investigations of wurtzite-phase ZnMgO nanopowders synthesized by ball-milling, Phys. B Condens. Matter 604 (2021) 412735, https://doi.org/10.1016/j.physb.2020.412735.

[9] L. Xia, Zh Liu, P. Taskinen, Solubility study of the halite and wurtzite solid solutions in the MgO-ZnO system within temperature range from 1000-1600 °C, J. Alloys Compd. 687 (2016) 827–832, https://doi.org/10.1016/j.jallcom.2016.06.191.
[10] F. Greuter, Electrically active interfaces in ZnO varistors, Solid State Ionics 75 (1995) 67–78, https://doi.org/10.1016/0167-2738(94)00181-Q.
[11] J.L. Morrison, J. Huso, H. Che, D. Thapa, M. Huso, M. Grant Norton, L. Bergman, The formation of MgZnO luminescent ceramics, J. Mater. Sci. Mater. Electron. 23 (2012) 437–444, https://doi.org/10.1007/s10854-011-0530-7.
[12] J. Zhang, F. Pan, W. Hao, T. Wang, Effect of MgO doping on the luminescent properties of ZnO, Mater. Sci. Eng. B 129 (2006) 93–95, https://doi.org/10.1016/j.mseb.2005.12.028.
[13] Amit K. Das, P. Misra, R.S. Ajimsha, A. Bose, S.C. Joshi, S. Porwal, T.K. Sharma, S.M. Oak, L.M. Kukreja, Effect of Mg diffusion on photoluminescence spectra of MgZnO/ZnO bi-layers annealed at different temperatures, J. Appl. Phys. 114 (2013) 183103, https://doi.org/10.1063/1.4830010.
[14] M. Xue, Q. Guo, K. Wu, J. Guo, Initial oxidation and interfacial diffusion of Zn on faceted MgO(111) films, Langmuir 24 (2008) 8760–8764, https://doi.org/10.1021/la801314s.
[15] R.S. Wang, H.C. Ong, Study of interfacial diffusion in Al_2O_3/ZnO and MgO/ZnO heterostructures, J. Appl. Phys. 104 (2008) 016108, https://doi.org/10.1063/1.2952505.
[16] F.E. Dart, Evaporation of zinc and zinc oxide under electron bombardment, Phys. Rev. 78 (1950) 761–764, https://doi.org/10.1103/PhysRev.78.761.
[17] N.O. Korsunska, L.V. Borkovska, B.M. Bulakh, L. Yu Khomenkova, V.I. Kushnirenko, I.V. Markevich, The influence of defect drift in external electric field on green luminescence of ZnO single crystals, J. Lumin. 102–103 (2003) 733–736, https://doi.org/10.1016/S0022-2313(02)00634-8.
[18] S. Wang, Y. Wang, Q. Ramasse, Z. Fan, The nature of native MgO in Mg and its alloys, Metall. Mater. Trans. A 51 (2020) 2957–2974, https://doi.org/10.1007/s11661-020-05740-1.